



# Confinement effects on energy harvesting by a heaving and pitching hydrofoil

Yunxing Su<sup>\*</sup>, Michael Miller, Shreyas Mandre, Kenneth Breuer

School of Engineering, Brown University, Providence, RI 02912, USA



## HIGHLIGHTS

- The highest efficiency of energy harvesting is up to 50% under wall confinement.
- The increased hydrodynamic forces are responsible for the efficiency improvement.
- The enhanced force is due to the flow blockage by the walls and the hydrofoil.
- The optimal pitch amplitude and reduced frequency increase with confinement.

## ARTICLE INFO

### Article history:

Received 7 April 2018

Received in revised form 7 October 2018

Accepted 8 November 2018

Available online 22 November 2018

### Keywords:

Renewable energy

Oscillating hydrofoil

Wall confinement effect

Power extraction

Leading-edge vortex

## ABSTRACT

Wall confinement effects on the energy harvesting performance by a flapping hydrofoil (aspect ratio = 4.5) have been investigated in a circulating water flume at a Reynolds number of 50,000. Measurements of hydrodynamic forces are taken for three different confinement configurations (unconfined, one-wall and two-wall confinement) and a series of confinement levels for each configuration. Compared with the unconfined situation, a significant improvement of efficiency performance is obtained for strong two-wall confinement due to the enhancement of the hydrodynamic forces, while only a modest increase is observed in the one-wall confinement configuration. Results show that the heave component of efficiency is the primary contributor to the performance improvement. A parametric study, varying reduced frequency and pitching amplitude, shows that as the confinement increases, the optimal energy harvesting occurs at larger values of the reduced frequency and pitching amplitude, and can reach a Lanchester–Betz efficiency as high as 50%.

© 2018 Elsevier Ltd. All rights reserved.

## 1. Introduction

Tidal and marine energy harvesting using flapping hydrofoils is receiving increasing interest in recent years as these energy harvesters are potentially more environmentally friendly and robust due to their low operating speeds (Xiao and Zhu, 2014; Young et al., 2014) as compared to conventional rotary turbines. McKinney and DeLaurier (1981) first studied the power extraction behavior of a harmonically flapping foil (“Windmill”) and demonstrated the feasibility of producing power from steady flows. Numerical simulations were reported (Jones and Platzer, 1997; Jones et al., 1999) to show good agreements with the Windmill experiments in terms of the efficiency of energy harvesting at low speeds and small angles of attack. The optimal efficiency of energy harvesting was explored numerically using a parametric sweep of the operating frequency,  $f$ , and pitching amplitude,  $\theta_0$ , and the highest efficiency was reported to reach 35% (Kinsey and Dumas, 2008). A

<sup>\*</sup> Corresponding author.

E-mail address: [yunxing\\_su@brown.edu](mailto:yunxing_su@brown.edu) (Y. Su).

more recent experimental study (Kim et al., 2017) on a heaving and pitching hydrofoil confirmed these results, and divided the power extracted by the hydrofoil into two parts: a heave component and a pitch component. The researchers found that the heave component of energy harvesting increased with the reduced frequency, while the pitch component turned from positive to negative at high reduced frequency, indicating that the pitching motion consumed energy rather than extracting energy from the flow. In addition to numerical simulations or lab-scale experiments, prototype field tests of the oscillating hydrofoil energy harvesters were performed (Kinsey et al., 2011; Mandre et al., 2015), successfully demonstrating the capability of energy extraction in realistic flow conditions.

Several efforts have focused on further improving the performance of power extraction by a flapping hydrofoil. Besides hydrofoil flexibility (Wu et al., 2015a) and using a tandem-foil configuration (Ashraf et al., 2011; Kinsey and Dumas, 2012; Broering et al., 2012; Karakas and Fenercioglu, 2017), another approach to potentially improving the power extraction performance of a flapping hydrofoil is to operate the hydrofoil close to a wall inside a channel and take advantage of the wall confinement effects as proposed by Zhu et al. (2008). Theoretical studies (Garrett and Cummins, 2005, 2007; Houlby et al., 2008; Whelan et al., 2009) have shown that the wall confinement effects can considerably increase the power extraction, rising above the so-called “Lanchester–Betz” limit of 59% for an unconfined rotary turbine (Lanchester, 1915; Betz, 1920; Van Kuik, 2007). In those studies, the Lanchester–Betz efficiency limit was increased by a factor of  $(1 - B)^{-2}$ , where  $B$  is the ratio between the frontal turbine area and the channel width.

Regarding wall confinement effects on an unsteady or flapping hydrofoil, the available data are mostly from numerical simulations. Computations of a heaving foil close to a wall (Moryossef and Levy, 2004; Molina and Zhang, 2011) showed enhanced lift force on the foil, which could potentially contribute to enhancing energy harvesting. More directly, numerical studies (Zhu et al., 2008; Wu et al., 2014) of the energy harvesting performance with a semi-passive flapping foil (prescribed pitching motion, but passive heaving motion) showed that a smaller clearance between the foil and the wall resulted in a higher efficiency of power extraction. As for the prescribed oscillating hydrofoils, power extraction output was reported to be improved in both one-wall confinement (Wu et al., 2015b) and two-wall confinement (Gauthier et al., 2016) configurations. In particular, Gauthier et al. (2016) pointed out that this improvement in performance could be attributed to the increase of the effective angle of attack, which led to a stronger leading-edge separation due to the flow acceleration around the hydrofoil caused by the wall confinement effects. It was reported (Wu et al., 2015b) that the heave component of power extraction was primarily responsible for such improvement in power extraction. Different from the monotonic efficiency increase predicted by Garrett and Cummins (2007), a recent experimental study on two-wall confinement effects (Karakas and Fenercioglu, 2016) reported a maximum increase in efficiency by 43.50% at a foil-wall distance of 1 chord. With the help of the Particle Image Velocimetry (PIV) measurements, Karakas and Fenercioglu (2016) attributed this efficiency increase to the extended residence of leading-edge vortex (LEV) on the suction side of the hydrofoil due to the wall confinement. Similarly, the numerical counterpart (Hoke et al., 2017) to the experimental study reported an optimal foil-wall distance of 0.5 chord with an efficiency increase of 28%. Nonetheless, the authors further pointed out that, since only one set of parameters had been investigated, a larger range of operating parameters was needed to optimize the energy harvesting performance under wall confinement.

All (but one) of the aforementioned studies on energy harvesting with confined environment are based on theoretical analysis or CFD simulation; more experimental data are needed to find the optimal energy harvesting performance and analyze the connection between the wall confinement effects and the efficiency improvement. To address this, the present paper reports on experiments concerning the energy harvesting performance of a flapping hydrofoil in a free-surface water flume under three different confinement configurations: unconfined, one-wall and two-wall confinement. The confinement effects are analyzed by comparing the force and energy harvesting performance between the three configurations, with respect to the confinement levels and the contribution from heaving and pitching motions. Finally, a parametric study over the pitching amplitude and the motion frequency is presented to give a global picture of energy harvesting performance of an oscillating hydrofoil subject to wall confinement. The changes in the optimal operating parameters due to the wall confinement are then discussed.

## 2. Experimental setup

Fig. 1a illustrates the testing configuration, which consists of a hydrofoil with an elliptical cross section (chord,  $c = 0.1$  m, span,  $b = 0.45$  m, maximum thickness,  $\delta = 0.008$  m) mounted vertically in a free-surface water flume (test section: width,  $W = 0.8$  m, depth,  $D = 0.6$  m). The hydrofoil can execute computer-controlled heaving and pitching motions (Fig. 1b). The heaving motion (perpendicular to the oncoming flow) is driven by a linear servo motor (AeroTech BLM-142-A-AC-H-S-5000), and the pitching motion employs a rotary stepper motor (D600, Applied Motion Products). The freestream velocity (magnitude  $U$ , density  $\rho$ , viscosity,  $\mu$ ) was measured using an Acoustic Doppler Velocimeter (Vectrino, Nortek AS) positioned upstream of the hydrofoil. The Reynolds number of the experiments, based on the chord of the hydrofoil,  $Re = \rho Uc / \mu$ , is approximately 50,000 (freestream velocity  $U$  about 0.5 m/s).

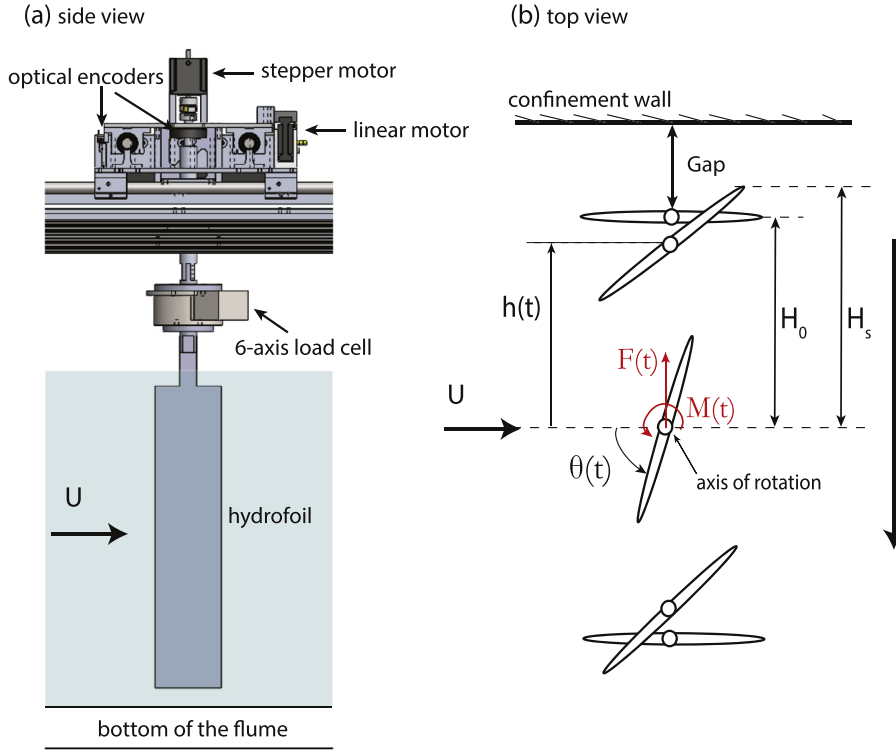


**Fig. 1.** (a) Side view of the experimental system in the water flume: The hydrofoil is mounted to the force transducer, which is attached to the shaft of the rotary stepper motor on the traverse stage driven by a linear motor; instantaneous motion positions are measured by optical encoders on the shaft of the stepper motor and on the rail of the linear motor, respectively; (b) top view of the heaving and pitching hydrofoil in the downstroke of the cycle with the pitching pivot at the mid-chord.  $h(t)$  and  $\theta(t)$  are the instantaneous heaving position and pitching angles, respectively;  $H_0$  is the heaving motion amplitude;  $H_s$  is the maximum swept distance of the hydrofoil; hydrodynamic forces (lift  $F(t)$  and torque  $M(t)$ ) on the hydrofoil are measured by the 6-axis load cell.

The prescribed pitching position,  $\theta(t)$ , and heaving position,  $h(t)$ , of the hydrofoil are defined as

$$\theta(t) = -\theta_0 \sin(2\pi ft), \quad (1)$$

and

$$h(t) = H_0 \sin(2\pi ft - \phi), \quad (2)$$

where  $\theta_0$  and  $H_0$  are the amplitudes of the pitching and heaving motions, respectively;  $f$  is the frequency for both the two motions. The phase difference,  $\phi$ , between the two motions was fixed at  $\pi/2$ , corresponding to the value for the optimal energy harvesting performance when the pitching axis is at the mid chord (McKinney and DeLaurier, 1981; Davids, 1999; Zhu, 2011). The reduced frequency is defined as:  $f^* = fc/U$ .

The instantaneous status of the heaving motion,  $h(t)$ , and the pitching motion,  $\theta(t)$ , were recorded by encoders on the heaving rail and on the rotating shaft, respectively. The hydrodynamic lift force,  $F(t)$  (perpendicular to the flow direction), and torque,  $M(t)$  (about the pitch axis), on the hydrofoil were directly measured using a 6-axis load cell (ATI IP65) mounted on the shaft of the hydrofoil above the water line (Fig. 1a). The lift force and the torque signals were acquired immediately following the initiation of the hydrofoil's motion. The first 3 cycles were ignored in the data analysis, and phase-averaging of the data was performed using the following 10 cycles with a standard deviation smaller than 6% of the mean value (same as in Kim et al. (2017)). The non-dimensional lift and torque coefficients,  $C_f$ , and  $C_m$  are defined as

$$C_f = \frac{F(t)}{0.5\rho U^2 cb}, \quad (3)$$

and

$$C_m = \frac{M(t)}{0.5\rho U^2 c^2 b}. \quad (4)$$

The instantaneous power extracted from or put into the flow,  $P(t)$ , is calculated from the measured lift, torque and the corresponding velocities,  $\dot{h}(t)$  and  $\dot{\theta}(t)$ :

$$P(t) = F(t)\dot{h}(t) + M(t)\dot{\theta}(t). \quad (5)$$

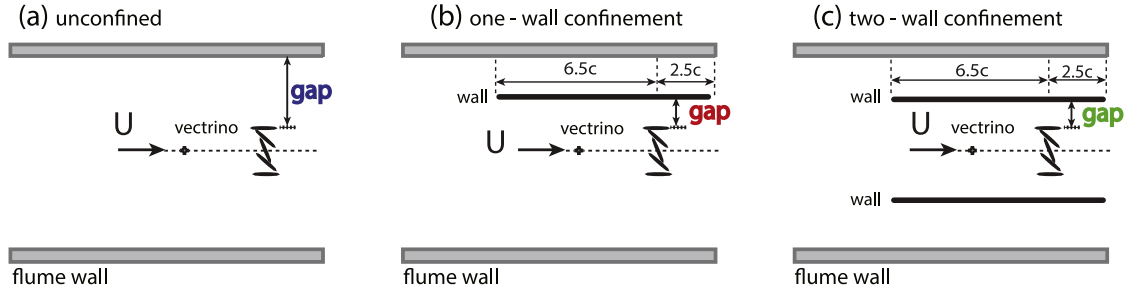


**Fig. 2.** Top view of three confinement configurations in the flume: (a) the unconfined configuration with no extra walls presented in the flume; (b) the one-wall confinement with only one wall installed in close proximity to the operating hydrofoil; (c) the two-wall confinement with two walls installed symmetrically on both sides of the operating hydrofoil. The gap value,  $g/c$ , is defined as the ratio of the minimum distance between foil shaft and the confinement wall(s) and the hydrofoil chord.

The Betz efficiency is defined as the ratio of the extracted power to the total energy flux available for extraction:

$$\eta = \frac{\langle P(t) \rangle}{0.5\rho U^3 A_s}, \quad (6)$$

where  $A_s = 2H_s b$  is the swept area of the hydrofoil and  $\langle P(t) \rangle$  is the power averaged over a full cycle (note that  $2H_s b$  is generally larger than  $2H_0 b$  since the pitching motion increases the swept area as shown in Fig. 1b). Since the power,  $P(t)$ , consists of two parts, the efficiency can also be divided into a heave component,  $\eta_h = \langle F(t)\dot{h}(t) \rangle / P_o$ , and a pitch component,  $\eta_p = \langle M(t)\dot{\theta}(t) \rangle / P_o$ , where  $P_o = 0.5\rho U^3 A_s$ .

### 2.1. Wall confinement configurations

As shown in Fig. 2, three confinement configurations were investigated during the experiments: unconfined, one-wall confinement, and two-wall confinement. These were achieved by placing extended wall(s) in proximity to the hydrofoil. To ensure accurate determination of the scaling parameters, the freestream velocity was always measured upstream of the hydrofoil with the Vectrino positioned inside the channel formed by the confinement wall(s). For the unconfined case, the maximum blockage ratio (the ratio between the hydrofoil area and the flume test section area, is 10%. However, this is only realized at the instant of maximum pitch amplitude, and the time-averaged blockage ratio is 6.4% for a pitch amplitude of  $90^\circ$ . Previous work Kim et al. (2017) using the same experimental facility reported that forces measured with a foil of chord  $b = 0.075$  m, were indistinguishable from the forces measured with a foil of chord length of  $c = 0.1$  m. Based on this, we are confident that the results of the ‘unconfined’ configuration in the present case is accurate. The results presented will also confirm this assertion.

A non-dimensional gap,  $g/c$ , was introduced to represent the confinement level, defined as the ratio between the minimum distance achieved from the shaft of the hydrofoil to the confinement wall(s) and the chord of the foil (Fig. 2). Smaller values of  $g/c$  correspond to stronger wall confinement levels. In the present study,  $g/c$  ranged from 3.2 (the unconfined configuration) to 0.5 (the highest confinement level) in both one-wall and two-wall confinement configurations.

## 3. Results and discussion

### 3.1. Hydrodynamic forces and efficiency

To investigate the hydrodynamic force and the resulting instantaneous energy harvesting performance for different wall confinement configurations, the kinematic parameters of reduced frequency, pitching and heaving amplitudes were fixed at  $f^* = 0.145$ ,  $\theta_0 = 75^\circ$ , and  $H_0/c = 0.8$ . Fig. 3 shows the lift coefficient  $C_f$  (a) and the torque coefficient  $C_m$  (b), and the corresponding instantaneous efficiency (c) and (d) for the unconfined (blue), one-wall (red) and two-wall (green) configurations at a moderate confinement level of  $g/c = 0.8$ . The motion of the hydrofoil with respect to the uniform flow direction is shown in the cartoon in Fig. 3a together with the wall location in the one-wall configuration. Five specific timings in the hydrofoil motion are marked out for both the upstroke and downstroke.

In the case of the unconfined configuration during the upstroke ( $t/T = 0$  to  $0.5$ ), the hydrodynamic lift force increases from a slightly negative value at pitching angle  $\theta = 0$  (geometric angle of attack) to its first peak before  $t/T = 0.25$ , during which the hydrodynamic lift force is recovered by the increase of geometric angle of attack. After the first peak, the slight decrease in lift is probably due to the beginning of the leading-edge separation at a large geometric angle of attack near  $t/T = 0.25$ . From  $t/T = 0.25$  to  $0.4$ , the growing in strength of the leading-edge vortex (LEV) presumably leads to the second peak in the lift force curve. The LEV is shed from the hydrofoil and the lift force drops quickly as the geometric angle of attack decreases to zero. This behavior of the lift force enhanced by LEV formation is supported by the results of McCroskey

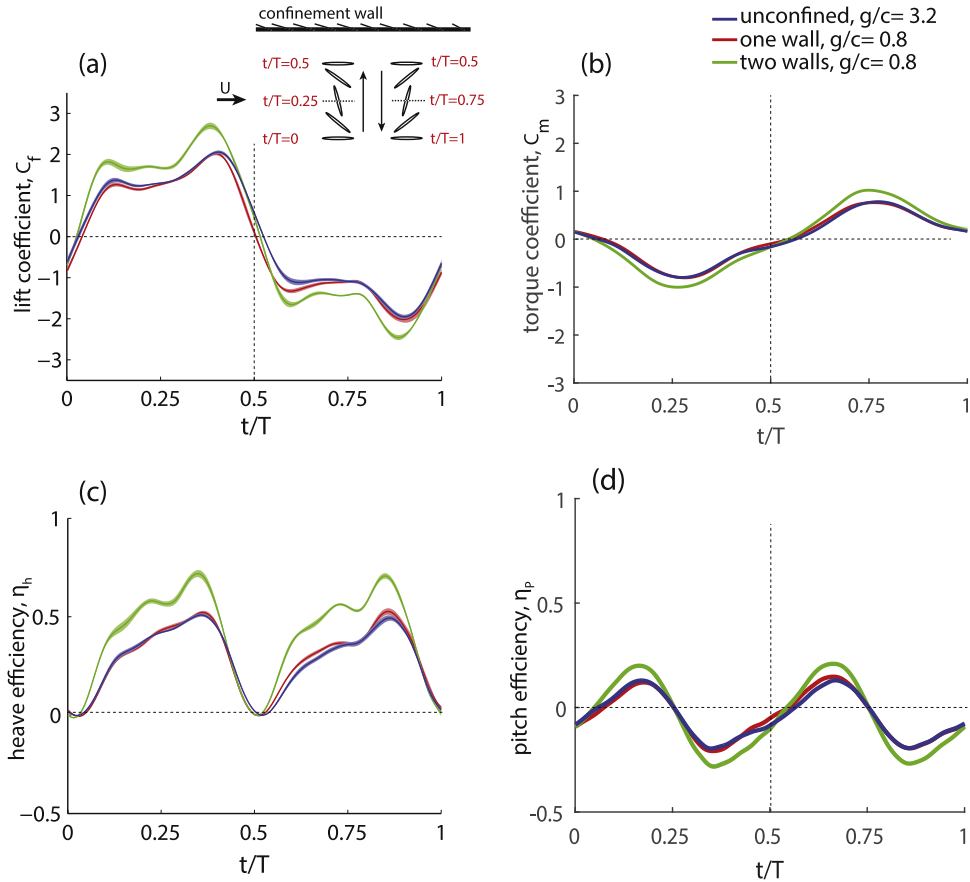


**Fig. 3.** Instantaneous hydrodynamic forces: (a) lift coefficient  $C_f$  and (b) torque coefficient  $C_m$ ; instantaneous efficiency of energy harvesting: (c) heave component  $\eta_h$  and (d) pitch component  $\eta_p$ , at reduced frequency  $f^* = 0.145$ , pitching amplitude  $\theta_0 = 75^\circ$  and heaving amplitude  $H_0/c = 0.8$ , with confinement level  $g/c = 0.8$  for both one-wall configuration (red curves) and two-wall configuration (green curves), and blue curves for unconfined configuration ( $g/c = 3.2$ ) as reference. The width of the curves denotes the standard deviation of the measured data.

(1982), Milano and Gharib (2005) and Kim et al. (2017), who investigated the connection between the vortex dynamics and the hydrodynamic force production on a foil. The authors reported that the maximum lift force was achieved when the circulation of the vortex saturated and that the lift force decreased due to the subsequent vortex shedding, consistent with the results in the current study.

Meanwhile, the hydrodynamic torque in the unconfined configuration demonstrates a simple temporal evolution throughout the cycle (Fig. 3b), with a monotonic increase ( $t/T = 0$  to  $0.3$ ) and decrease ( $t/T = 0.3$  to  $0.5$ ) during the upstroke. It should be noted that the timing of the drop in torque ( $t/T \sim 0.3$ ) happens earlier than the drop in the lift force ( $t/T \sim 0.4$ ) during the upstroke ( $t/T = 0 - 0.5$ ). This early decrease in torque resonates with the observation from Onoue and Breuer (2016) who associated the evolution of torque on a flapping flat plate to the relative location of the vortex core with respect to the pivot axis. The authors pointed out that the change in the location of the LEV, instead of the vortex shedding that happened a little later, was responsible for the decrease of the hydrodynamic torque on the flapping plate. After the pitch reversal at  $t/T = 0.5$ , the hydrofoil then experiences symmetric hydrodynamic forces and torques during the downstroke ( $t/T = 0.5 - 1$ ).

In the case of one-wall confinement (red curve in Fig. 3), the force and torque behaviors are very similar to the unconfined case. However, there is a slight increase in the lift force immediately after the pitch reversal as the foil begins the downstroke and moves away from the wall ( $t/T > 0.5$ ). In contrast, for the case of two-wall confinement (green curve in Fig. 3), a significant enhancement in hydrodynamic lift and torque coefficients is observed during both the upstroke and the downstroke. This suggests that the mechanisms that lead to the force enhancement in the one-wall case are acting near both  $t/T = 0$  and  $t/T = 0.5$  since the foil under two-wall confinement is moving away from a wall at both these points during the cycle. Therefore, the LEV that forms on both the upstroke and the downstroke is stronger. As shown in Fig. 3a, the peak force occurs a little earlier in the cycle in the confined configuration than in the unconfined, suggesting that the LEV separates from the foil a little earlier in the confined configuration. This will become important in Section 3.3 when we discuss the changes in optimal frequency due to the confinement effects.

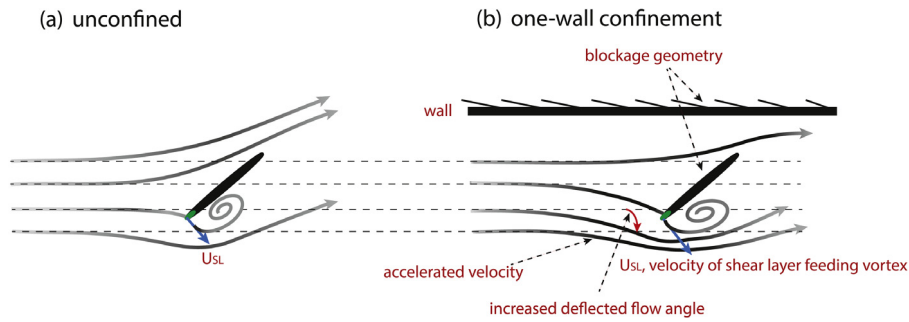


**Fig. 4.** Demonstration of streamlines near the hydrofoil at the beginning of the downstroke: (a) the unconfined configuration and (b) the one-wall confinement. The velocity and in-coming flow angle increase near the leading edge in the one-wall confinement due to the flow deflection by the wall.

As shown in Fig. 3c, similar trends in the instantaneous phase-averaged efficiency of power extraction are observed in the one-wall and two-wall confinements. To be specific, the changes in the heave efficiency between the unconfined and the one-wall confinement are small during the upstroke ( $t/T = 0$  to  $0.5$ ), but a modest efficiency increase can be observed right after  $t/T = 0.5$  with the hydrofoil moving away from the wall. This matches the increase observed in the hydrodynamic lift force. The change in efficiency is only modest because the foil is moving quite slowly during this part of the cycle and so the contribution to power is small. However, for the case of two-wall confinement, the efficiency is enhanced over the entire cycle.

It is noted that the heave efficiency (Fig. 3c) remains positive throughout the cycle regardless of the confinement configuration, while the pitch efficiency (Fig. 3d) is positive (extracting energy from the mean flow) during the first and third quarters of the cycle and negative (imparting energy into the flow) during the second and fourth quarters of the cycle. However, the amount of energy gain and loss in the pitch efficiency are not quite balanced, with more energy lost than gained. This negative net efficiency is attributed to the asymmetric torque history, with the peak in torque shifting to the second half of the upstroke ( $t/T = 0.25 - 0.5$ , Fig. 3b). This hydrodynamic torque performance is similar to the results discussed by Kim et al. (2017) who, with the help of PIV measurements, observed that a negative pitch efficiency at high reduced frequency was due to the asymmetric hydrodynamic torque performance caused by the extended residence of LEV on the hydrofoil.

### 3.1.1. The role of the effective angle of attack

The improvement of hydrodynamic forces and instantaneous efficiency in the two-wall confinement, as discussed by Gauthier et al. (2016), can be understood with reference to an increase in the effective angle of attack (AOA),  $\theta_e$ :

$$\theta_e(t) = \theta(t) - \arctan\left(\frac{\dot{h}(t)}{U}\right). \quad (7)$$

The effective AOA takes into account both the physical AOA and the contribution by the heaving velocity  $\dot{h}(t)$ . Using this, the force enhancement created by the confinement in the one-wall configuration can be attributed to the asymmetric local velocity profiles caused by different channel geometries formed by the hydrofoil and the installed wall during the upstroke and downstroke. Specifically, at the start of the downstroke (Fig. 4b), a flow blockage is created by the geometry formed by the rotated hydrofoil and the wall. Owing to this blockage, the fluid flow, which would be deflected toward the trailing edge of the hydrofoil if there were no wall presented (Fig. 4a), is now partly deflected toward the leading edge of the hydrofoil due to the presence of the wall near the trailing edge (Fig. 4b). This deflected flow toward the leading edge can potentially lead to two major changes in the flow conditions that the hydrofoil perceives: one is the acceleration of the local flow speed near the leading edge of the hydrofoil; the other is the change of the oncoming flow angle seen by the hydrofoil (Fig. 4b).

Both of these changes lead to increasing the effective AOA (Eq. (7)) and enhancing the feeding shear-layer velocity,  $U_{SL}$ . Although we do not present velocity measurements, previous results (Baik et al., 2012; Kim et al., 2017, e.g.) show that for a foil in uniform flow and at any appreciable angle of attack, flow separation and a “separating shear layer” form at the leading edge. The roll-up of this shear layer, which can be characterized by the velocity,  $U_{SL}$ , leads to the formation of the leading edge vortex (LEV) (schematically shown in Fig. 4). The vorticity flux in the shear layer feeds the circulation in the LEV and causes it to grow in size and strength. The feeding shear layer velocity,  $U_{SL}$ , has been found to be an important scaling parameter for the vortex growth (Dabiri, 2009; Sattari et al., 2012; Onoue and Breuer, 2016, 2017). An increase in  $U_{SL}$  leads to an increase in the growth rate of the LEV, resulting in a higher hydrodynamic force occurring earlier in the flapping cycle (Rival et al., 2009; Baik et al., 2012). This is in line with the observations of the hydrodynamic forces in the current study (Fig. 3a).

In contrast, during the upstroke in the one-wall confinement case, the geometry formed by the hydrofoil and the wall fails to introduce this additional blockage to the flow; thus the alteration of the local flow near the leading edge of the hydrofoil is small, resulting in negligible changes in the forces and torques compared with those in the unconfined configuration ( $t/T = 0 - 0.5$ , Fig. 3). This local alteration of the flow field in the immediate vicinity of the hydrofoil was also observed

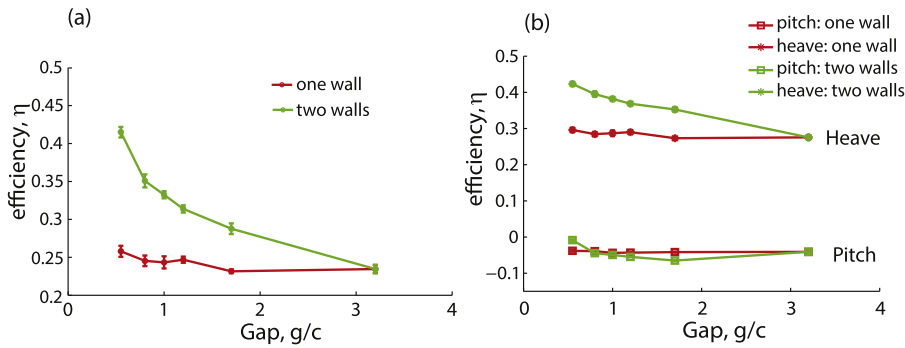


**Fig. 5.** Efficiency of energy harvesting under different confinement levels ( $g/c$ ): (a) total efficiency of energy harvesting,  $\eta$ , under one-wall (red curve) and two-wall (green curve) confinement; (b) heave component (square dots) of efficiency and pitch component (star dots) of (a). Operating parameters of the hydrofoil: reduced frequency  $f^* = 0.145$ , pitching amplitude  $\theta_0 = 75^\circ$  and heaving amplitude  $H_0/c = 0.8$ . Unconfined case corresponds to one single data point at  $g/c = 3.2$  as reference.

in the numerical simulations by Gauthier et al. (2016) and also contributed to a change in the effective AOA and the energy harvesting performance between the upstroke and the downstroke, similar to that observed here.

In the case of two-wall confinement, the flow blockage formed by the hydrofoil and the wall is achieved during both the upstroke and the downstroke portions of the cycle. Additionally, the local flow acceleration near the leading edge of the hydrofoil due to the blockage geometry is amplified in the two-wall confinement based on the fact that the hydrodynamic forces and the instantaneous efficiency of energy harvesting experience more substantial enhancement in the two-wall confinement (green curve) than in the one-wall confinement (red curve) as shown in Fig. 3a. This amplification effect in the local flow velocity in the two-wall configuration is reasonable considering the complete constraint of the flow in a channel of finite width formed by the walls. Furthermore, the blockage geometry formed by the hydrofoil and the wall(s) in two-wall confinement increases the constraint of the fluid flow by adding additional blockage in the channel of finite width. This additional blockage, which is related to the pitching angle of the hydrofoil, will be important in Section 3.3 in the discussion of changes in the optimal pitching amplitude.

### 3.2. Dependence on gap, $g/c$

To investigate the connection between the power extraction performance and the confinement levels,  $g/c$ , the energy harvesting efficiency was measured at a series of confinement levels in both the one-wall (red curves) and two-wall (green curves) configurations (Fig. 5). As before, the frequency, pitching and heaving amplitudes are kept constant,  $f^* = 0.145$ ,  $\theta_0 = 75^\circ$ ,  $H_0/c = 0.8$ . In the one-wall configuration, the energy harvesting efficiency shows only a limited improvement even at high confinement levels (small  $g/c$ ) with the efficiency increasing from 24% at the unconfined configuration to around 26% at the highest confinement.

By contrast, a significant increase in efficiency is observed in the two-wall configuration, rising from approximately 24% in the unconfined configuration ( $g/c = 3.2$ ) to 42% at the highest confinement level ( $g/c = 0.5$ ). This notable improvement is reasonable considering the large augmentation in the lift force and the resulting instantaneous efficiency (green curves in Fig. 3a,c) in the two-wall configuration. This enhancement in the energy harvesting performance is also seen in the results in Garrett and Cummins (2007), Karakas and Fenercioglu (2016) and Hoke et al. (2017), who also attributed the enhancement in energy harvesting performance to the flow acceleration around the hydrofoil due to the wall confinement.

The total efficiency of the power extraction can be divided into the heave component and pitch component, as discussed by Kim et al. (2017). Fig. 5b shows the contribution to the total efficiency from the heaving and pitching motions in both the one-wall (red curve) and two-wall (green curve) configurations. In the one-wall configuration, though the overall improvement is limited, this small improvement mainly comes from the heave component and can be associated with the modest change in the lift force (red curve in Fig. 3a) that occurs when the foil moves away from the wall and forms a blockage geometry that deflects and accelerates the local flow near the leading edge (Fig. 4b). However, this flow modification is small and limited to the moment right after the pitch reversal. Since the heaving velocity right after the pitch reversal is low, the overall improvement in efficiency is small. In the two-wall configuration, as discussed in Section 3.1, only positive improvement can be achieved from the confinement effects. The observations of the heave efficiency in Fig. 5b confirm the results from Section 3.1 that the efficiency improvement due to the confinement effects mainly come from the heave component.

### 3.3. Optimal reduced frequency, $f^*$ , and pitching amplitude, $\theta_0$

As we have already seen, the two-wall confinement can significantly improve the energy harvesting efficiency at a given combination of operating frequency,  $f^*$ , and pitching amplitude,  $\theta_0$ . In this section, we explore the changes in the

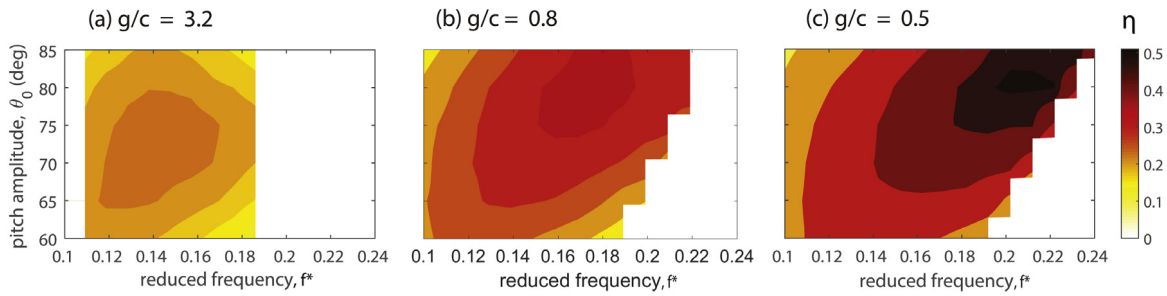


**Fig. 6.** Contours of efficiency as functions of reduced frequency  $f^* = fc/U$  and pitching amplitude  $\theta_0$  at three (two-wall) confinement levels. (a)  $g/c = 3.2$  (unconfined configuration); (b)  $g/c = 0.8$ ; (c)  $g/c = 0.5$ . The heaving amplitude remains  $H_0/c = 0.8$  for all the cases above. The location of the efficiency peak in the contour shifts to the top right corner when decreasing the gap values, corresponding to higher reduced frequency and pitching amplitude.

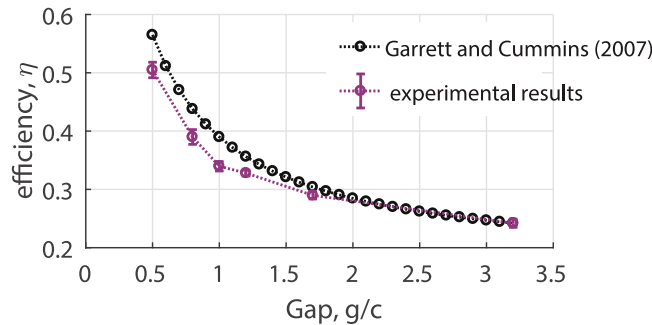


**Fig. 7.** Comparison in efficiency between the prediction by [Garrett and Cummins \(2007\)](#) and the optimal efficiency measured at each confinement level.

optimal parameters,  $f^*$  and  $\theta_0$ , under two-wall confinements. [Fig. 6](#) shows the energy harvesting efficiency vs  $f^*$  and  $\theta_0$  for three different confinement levels:  $g/c = 3.2, 0.8$  and  $0.5$ . In all cases the heaving amplitude,  $H_0/c$ , remains fixed at  $0.8$ . Generally, one can see that the maximum efficiency increases with the confinement level and that the location of the optimal performance in the parameter space shifts to the top right corner, with a larger reduced frequency and a larger pitching amplitude. To be specific, in the unconfined configuration ([Fig. 6a](#)), the highest efficiency is about  $0.25$ , located at  $f^* = 0.14$  and  $\theta_0 = 70^\circ$ , in good agreement with previous results ([Kinsey and Dumas, 2008](#); [Zhu et al., 2008](#); [Kim et al., 2017](#)). When the confinement level rises to  $g/c = 0.8$ , the maximum efficiency increases to a value of approximately  $0.35$ , achieved using both a higher reduced frequency ( $f^* = 0.17$ ) and pitching amplitude ( $\theta_0 = 75^\circ$ ) ([Fig. 6b](#)). At the highest confinement level of  $g/c = 0.5$  ([Fig. 6c](#)), the energy harvesting performance is further enhanced, with the peak efficiency of approximately  $0.5$ , occurring for values of  $f^*$  and  $\theta_0$  of about  $0.2$  and  $80^\circ$ , respectively.

The shift in the optimal reduced frequency can be attributed to the change in the phase of the maximum lift force that occurs due to the confinement effects. As seen in [Fig. 3](#) (Section 3.1), at a fixed reduced frequency, the peak of the lift force appears earlier in the heaving cycle when the hydrofoil is confined, indicating a faster vortex growth rate and an earlier vortex shedding from the hydrofoil in the confined configuration. As was commented earlier, the faster vortex growth is likely due to the higher local velocity induced by the confinement ([Fig. 4](#)), and suggests that in order to maintain the optimal synchronization between the lift force and the heave velocity a higher reduced frequency is required. In addition, the higher reduced frequency can serve to stabilize the LEV. In experiments of leading-edge vortex growth on a heaving and pitching plate, [Baik et al. \(2012\)](#) showed that the increase in reduced frequency resulted in a reduction in the LEV growth rate while [Onoue and Breuer \(2017\)](#) also pointed out that a larger reduced frequency (resulting in a larger centrifugal force) contributed to the delayed vortex detachment by diminishing the axial drifting of the vortex core.

The effective angle of attack (AOA) discussed in Section 3.1 is also critical in increasing the hydrodynamic forces and thus the performance of energy harvesting. With the increase in the optimal reduced frequency, the heaving velocity rises. The pitching amplitude must therefore also increase, in order to maintain an optimal effective angle of attack (Eq. (7)). This trend is observed in [Fig. 6a–c](#). The higher pitching amplitude also has the effect of increasing the local flow blockage and hence increasing the local flow velocity ([Fig. 4](#)), further improving the overall energy harvesting performance.

As discussed by [Garrett and Cummins \(2007\)](#), the Lanchester–Betz efficiency limit ( $16/27 = 0.593$ ) for an unconfined turbine (actuator disk) increases by a factor of  $(1 - A/A_c)^{-2}$  for a turbine of cross section  $A$  in a finite width channel of cross section  $A_c$ . Although we cannot make a direct comparison, since the Betz efficiency of a rotary turbine is different from the peak efficiency of the pitching and heaving hydrofoil, we can nevertheless test the trend. To do so, we compare the optimal efficiency achieved in the experiments at each confinement level with the theoretical prediction:  $\eta_o(1 - A/A_c)^{-2}$ , where  $\eta_o$  is the experimentally-measured peak efficiency of the hydrofoil operating in an unconfined flow,  $\eta_o = 0.25$ . [Fig. 7](#) shows this

comparison, and although Garrett and Cummins's prediction is generally higher than the experimentally-measured optimal efficiency, the overall trend is reproduced very well. The overestimation of efficiency from their model is not surprising considering the idealized assumptions of the model and the fact that it does not consider mixing in the wake.

#### 4. Conclusions

In the present study, we have explored the wall confinement effects on the energy harvesting performance of a heaving and pitching hydrofoil in a laboratory flume, extending previous theoretical and numerical studies. The results confirm the actuator disk theoretical predictions of Garrett and Cummins (2007), showing that the power extraction efficiency increases with the confinement level for both the one-wall and two-wall configurations. Specifically, a limited improvement in efficiency is seen in the one-wall configuration regardless of the confinement levels explored. However, a significant increase in efficiency is observed at high confinement levels in the two-wall configuration (the maximum efficiency is up to 50%). The phase-averaged force profiles, a result unique to the current work, suggest that the enhanced performance primarily comes from the increase of the hydrodynamic lift force due to the local velocity acceleration around the hydrofoil caused by the presence of the confinement walls. As the power loss by the pitching component remains small, a net increase in energy is achieved.

A parametric sweep of the reduced frequency and the pitching amplitude under different confinement levels reveals that the optimal parameters for energy harvesting shift with confinement. The optimal reduced frequency,  $f^*$ , and pitching amplitude,  $\theta_0$ , both increase as the confinement increases (smaller  $g/c$  values), a trend that can be understood in terms of adjusting the frequency and effective angle of attack to the higher local velocity that the foil experiences due to the proximity of the wall. The phase-averaged force measurements provide valuable insight regarding the formation, growth and separation of the leading edge vortex that is so critical to the performance of this class of devices. Nevertheless, velocity measurements would be extremely valuable to confirm our arguments. Experiments in this direction, using PIV, are forthcoming and will be reported in the near future.

#### Acknowledgments

The authors gratefully acknowledge financial support from Advanced Research Projects Agency-Energy, United States (ARPA-E award DE-AR0000318). In particular, we thank Jen Franck and other members of the Leading Edge team for their support and insight.

#### References

- Ashraf, M.A., Young, J., Lai, J.C.S., Platzer, M.F., 2011. Numerical analysis of an oscillating-wing wind and hydropower generator. *AIAA J.* 49, 1374–1386.
- Baik, Y.S., Bernal, L.P., Granlund, K., Ol, M.V., 2012. Unsteady force generation and vortex dynamics of pitching and plunging aerofoils. *J. Fluid Mech.* 709, 37–68.
- Betz, A., 1920. Das Maximum der theoretisch möglichen Ausnützung des Windes durch Windmotoren. *Z. Gesamte Turbinenwesen* 26, 307–309.
- Broering, T.M., Lian, Y., Henshaw, W., 2012. Numerical investigation of energy extraction in a tandem flapping wing configuration. *AIAA J.* 50, 2295–2307.
- Dabiri, J.O., 2009. Optimal Vortex Formation as a Unifying Principle in Biological Propulsion. *Annu. Rev. Fluid Mech.* 41, 17–33.
- Davids, S.T., 1999. A Computational and Experimental Investigation of a Flutter Generator. Thesis Dissertation of Naval Postgraduate School.
- Garrett, C., Cummins, P., 2005. The power potential of tidal currents in channels. *Proc. R. Soc. Lond. Ser. A Math. Phys. Eng. Sci.* 461, 2563–2572.
- Garrett, C., Cummins, P., 2007. The efficiency of a turbine in a tidal channel. *J. Fluid Mech.* 588, 243–251.
- Gauthier, É., Kinsey, T., Dumas, G., 2016. Impact of blockage on the hydrodynamic performance of oscillating-foils hydrokinetic turbines. *J. Fluids Eng.* 138, 91–103.
- Hoke, C., Young, J., Lai, J., Karakas, F., Zaloglu, B., Fenercioglu, I., 2017. Investigation of oscillating-foil power generation in constrained flow. *Procedia Eng.* 199, 3450–3455.
- Houlsby, G.T., Draper, S., Oldfield, M., 2008. Application of Linear Momentum Actuator Disc Theory to Open Channel Flow. Oxford University Research Archive.
- Jones, K.D., Davids, S., Platzer, M.F., 1999. Oscillating-wing power generation. In: 3rd ASME/JSME Joint Fluids Engineering Conference.
- Jones, K.D., Platzer, M.F., 1997. Numerical computation of flapping-wing propulsion and power extraction. AIAA Paper No. 97-0826, 35th AIAA Aerospace Sciences Meeting, Reno, Nevada, Jan. 1997.
- Karakas, F., Fenercioglu, I., 2016. Effect of side-walls on flapping-wing power-generation: an experimental study. *J. Appl. Fluid Mech.* 9, 2769–2779.
- Karakas, F., Fenercioglu, I., 2017. Effect of phase angle on tandem flapping-wing power generation. *Int. J. Energy Prod. Manage.* 2, 95–105.
- Kim, D., Strom, B., Mandre, S., Breuer, K., 2017. Energy harvesting performance and flow structure of an oscillating hydrofoil with finite span. *J. Fluids Struct.* 70, 314–326.
- Kinsey, T., Dumas, G., 2008. Parametric study of an oscillating airfoil in a power-extraction regime. *AIAA J.* 46, 1318–1330.
- Kinsey, T., Dumas, G., 2012. Optimal tandem configuration for oscillating-foils hydrokinetic turbine. *J. Fluids Eng.* 134, 103–113.
- Kinsey, T., Dumas, G., Lalande, G., Ruel, J., Méhut, A., Viarouge, P., Lemay, J., Jean, Y., 2011. Prototype testing of a hydrokinetic turbine based on oscillating hydrofoils. *Renew. Energy* 36, 1710–1718.
- Lanchester, F., 1915. A contribution to the theory of propulsion and the screw propeller. *Trans. Inst. Naval Archit.* 57, 98–116.
- Mandre, S., Franck, J., Breuer, K., Fawzi, A., Cardona, J., Miller, M.J., Su, Y., Medina, A., Loera Loera, C., Junquera, E., Simeski, F., Volkmann, K., Lorick, R., Cowles, S., Luiz Rocha Ribeiro, B., Winckler, S., Derecktor, T., 2015. Oscillating hydrofoils for tidal energy extraction: experiments, simulations and salt water field tests. AGU Fall Meeting Abstracts.
- McCroskey, W.J., 1982. Unsteady airfoils. *Annu. Rev. Fluid Mech.* 14, 285–311.
- McKinney, W., DeLaurier, J., 1981. The Windmill: An oscillating-wing windmill. *J. Energy* 5, 109–115.
- Milano, M., Gharib, M., 2005. Uncovering the physics of flapping flat plates with artificial evolution. *J. Fluid Mech.* 534, 403–409.
- Molina, J., Zhang, X., 2011. Aerodynamics of a heaving airfoil in ground effect. *AIAA J.* 49, 1168–1179.
- Moryossef, Y., Levy, Y., 2004. Effect of oscillations on airfoils in close proximity to the ground. *AIAA J.* 42, 1755–1764.

- Onoue, K., Breuer, S.K., 2016. Vortex formation and shedding from a cyber-physical pitching plate. *J. Fluid Mech.* 793, 229–247.
- Onoue, K., Breuer, S.K., 2017. A scaling for vortex formation on swept and unswept pitching wings. *J. Fluid Mech.* 832, 697–720.
- Rival, D., Prangemeier, T., Tropea, C., 2009. The influence of airfoil kinematics on the formation of leading-edge vortices in bio-inspired flight. *Exp. Fluids* 46, 823–833.
- Sattari, P., Rival, D.E., Martinuzzi, R.J., Tropea, C., 2012. Growth and separation of a start-up vortex from a two-dimensional shear layer. *Phys. Fluids* 24, 107102.
- Van Kuik, G.A.M., 2007. The Lanchester-Betz-Joukowski limit. *Wind Energy* 10, 289–291.
- Whelan, J.I., Graham, J.M.R., Peiró, J., 2009. A free-surface and blockage correction for tidal turbines. *J. Fluid Mech.* 624, 281–291.
- Wu, J., Qiu, Y.L., Shu, C., Zhao, N., 2014. Pitching-motion-activated flapping foil near solid walls for power extraction: A numerical investigation. *Phys. Fluids* 26, 083601.
- Wu, J., Wu, J., Tian, F.B., Zhao, N., Li, Y.D., 2015a. How a flexible tail improves the power extraction efficiency of a semi-activated flapping foil system: A numerical study. *J. Fluids Struct.* 54, 886–899.
- Wu, J., Yang, S.C., Shu, C., Zhao, N., Yan, W.W., 2015b. Ground effect on the power extraction performance of a flapping wing biomimetic energy generator. *J. Fluids Struct.* 54, 247–262.
- Xiao, Q., Zhu, Q., 2014. A review on flow energy harvesters based on flapping foils. *J. Fluids Struct.* 46, 174–191.
- Young, J., Lai, J.C.S., Platzer, M.F., 2014. A review of progress and challenges in flapping foil power generation. *Prog. Aerosp. Sci.* 67, 2–28.
- Zhu, Q., 2011. Optimal frequency for flow energy harvesting of a flapping foil. *J. Fluid Mech.* 675, 495–517.
- Zhu, Q., Haase, M., Wu, C.H., 2008. Modeling the capacity of a novel flow-energy harvester. *Appl. Math. Model.* 33, 2207–2217.